Copper(I) iodide coordination polymers with triazole substituted pyridine ligands: photophysical and electrical conductivity properties

Shivendu Mishra, Dilip Pandey, Kulbhushan Mishra, Lydie Viau, Abhinav Raghuvanshi

Copper(I) iodide coordination polymers with triazole substituted pyridine ligands: Photophysical and electrical conductivity properties

Shivendu Mishra[a], Dilip Pandey[a], Kulbhushan Mishra[b], Lydie Viau[c] and Abhinav Raghuvanshi*[a]

[a]*Department of Chemistry, Indian Institute of Technology Indore, 453552, Madhya Pradesh, India.* Email: r.abhinav@iiti.ac.in

[b]*Department of Physics, Indian Institute of Technology Indore, 453552, Madhya Pradesh, India.*

[c]*Université de Franche-Comté, CNRS, Institut UTINAM, F-25000 Besançon, France.*

Abstract

This work aims to synthesize multifunctional materials with tunable emission properties. To pursue this, three isomeric ligands; 2-(1H-1,2,4-triazol-1-yl)pyridine (**L^1**), 3-(1H-1,2,4-triazol-1-yl)pyridine (**L^2**) and 4-(1H-1,2,4-triazol-1-yl)pyridine (**L^3**) were reacted with CuI to afford three different coordination polymers, $[Cu_2(\mu_3\text{-}I)_2(L^1)_2]_n$ **CP1**, $[Cu_2(\mu_2\text{-}I)_2(L^2)_2]_n$ **CP2** and $[Cu(\mu_2\text{-}I)(L^3)]_n$ **CP3**, respectively. **CP1** consists of a 1D chain comprising double-stranded Cu_2I_2 secondary building units (SBUs), where each copper is coordinated with triazolyl nitrogen of the ligand on each side of the chain while pyridine nitrogen remains pendant. Contrary to this, both pyridine and triazolyl nitrogens of **L^2** and **L^3** coordinate to Cu to give 1D and 2D, **CP2** and **CP3,** respectively. **CP2** has a discrete Cu_2I_2 rhomboid SBU bridged by two **L^2** ligands, whereas **CP3** has Cu-I single chains bridged by two **L^3** ligands to give a 2D sheet structure. All three coordination polymers are emissive at room temperature with emission colour varying from green and yellow to orange with a λ_{max} of 538, 568 and 600 nm, respectively for **CP1** to **CP3**.

CP1 and **CP3** show luminescence thermochromism on lowering the temperature from 298K to 77K, changing hues from green to blue and orange to yellow, respectively. In addition to unique emission properties, these CPs exhibit semiconductor behaviour, with electrical conductivity in the range of 10^{-7} S cm^{-1}. It is proposed that the presence of Cu_2I_2 double-stranded chain provides a better and continuous overlap of Copper and Iodine orbital giving better conductivity to **CP1** compared to **CP2** and **CP3**.

Keywords: Copper(I), triazole, coordination polymers, luminescence, electrical conductivity.

Introduction

Over the past few years, there has been significant progress in the development of multifunctional luminescent materials. In this context, inorganic-organic hybrid materials and complexes with a metal having d^{10} electronic configuration have been widely reported because of their interesting photophysical properties due to non-quenching of the excited state energy levels.[1–7] Particularly, copper(I) complexes are subjected to extensive study for their practical application in organic light-emitting diodes, light-emitting electrochemical cells, biological sensors, molecular wires, non-linear optics, electrically conductive materials, thermochromic sensors etc.[8–14] Complexes and coordination polymers (CPs) derived from copper(I) iodide with nitrogen, sulphur and phosphorous-containing ligands have emerged as promising candidates for multifunctional materials with variable photophysical and electrical properties and provide an alternative way to synthesize affordable and environmentally benign materials.[15–21] Furthermore, the structural diversity of copper halide complexes/CPs can also depend upon the coordinating ligands, metal-to-ligand ratios, and reaction conditions (temperature, pressure etc.).[22] The structural features significantly affect the electrical and photophysical properties of the complexes.[23,24] These complexes/CPs can have Cu-I single chain, Cu_2I_2 double chain, Cu_3I_3,

Cu_4I_4, Cu_8I_8 etc., type of SBUs that play an essential role in controlling the luminescent properties.[17,18,22,25,26] The luminescence properties of these molecules are dominated by the metal-to-ligand charge transfer (MLCT), metal and halide-to-ligand charge transfer (^{3}M+X-LCT), triplet cluster centered emission (^{3}CC) or combination of these charge transfer states.[27,28] In addition, the luminescence of copper(I) halide CPs may also respond to external stimuli such as temperature, pressure, pH etc., and show thermochromism, mechanochromism, vapochromism, aggregation induced emission (AIE) or solvatochromism.[29–34] In 1977, Hardt *et al.* reported the term fluorescence thermochromism, which refers to the change in luminescence with varying temperatures.[35] Ford *et al.* explained that the luminescence thermochromism in copper complexes (where the Cu--Cu distances in the clusters are less than the sum of van der Waals radii (i.e. 2.8Å)) is due to the presence of two emission bands; the higher energy band is assigned to halide to ligand charge transfer (^{3}XLCT) and the lower energy band attributed to triplet cluster-centered (^{3}CC) excited state localized at the copper cluster (SBU).[36]

Cu(I) polymers constructed with different ligands generally have a tetrahedral geometry around the Cu center, leading to the John-Teller flattening distortion in the excited state and suffering low quantum efficiency. Incorporating molecular rigidity on the ligands helps in reducing the non-radiative transitions, consequently improving the efficiency of the material.[37] *N*-containing multidentate ligands can act as a bridge between two centers offering the construction of 1D, 2D and 3D coordination polymers, leading to more rigidity in the resulting CPs.[38]

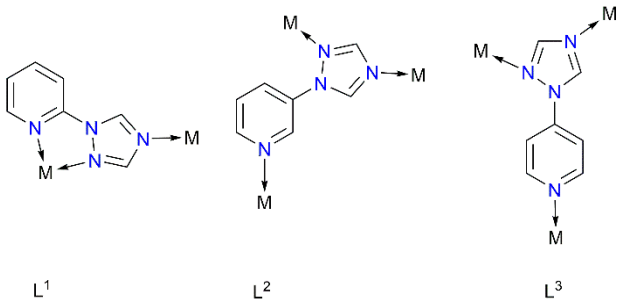

Fig. 1. Possible coordination modes in $\mathbf{L^1}$, $\mathbf{L^2}$ and $\mathbf{L^3}$.

Despite having multiple binding sites which could provide a better platform to generate CPs of varying dimensionality, 1,2,4-triazoles are relatively less explored for the formation of Cu(I) CPs. Zhu *et al*. have synthesized a luminescent copper(I) CP with ethyl-bridging bis(triazole) ligand featuring a Cu_4I_4 core and showing yellow emission at room temperature.[39] Baiyan *et al*. reported a series of copper coordination polymers based on amino-bis(pyridyl)-1,2,4-triazole showing luminescent properties.[40] Liu *et al*. reported a series of copper coordination polymer based on thiol and thione-functionalized 1,2,4-triazole having diverse luminescent properties.[41] Also, thethermochromic luminescence properties of copper(I) complexes with pyridine triazole and phosphine ligands have been reported.[42–45]

Considering these facts, we have chosen three different isomeric, molecularly rigid pyridine substituted 1,2,4-triazol-1-yl ligands $\mathbf{L^1}$, $\mathbf{L^2}$ and $\mathbf{L^3}$, having multiple coordinating sites at different positions (**Fig. 1)**. In this study, the reactivity of these ligands with copper(I) iodide has been explored. The photophysical properties of the resulting CPs have been investigated at room temperature (rt) and 77K. Further, the electrical conductivity of these CPs has also been measured, evidencing semiconductor properties of the CPs at room temperature.

Results and discussion

Ligands $\mathbf{L^1}$, $\mathbf{L^2}$ and $\mathbf{L^3}$ were synthesized by the reported procedures following Ullmann-type coupling reactions.[46–48] The ligand purity was confirmed by HPLC method by using acetonitrile (ACN) and water as a solvent mixture in isocratic mode (**Fig. S1-S2**). Three coordination polymers were synthesized by reacting copper(I) iodide and ligands in a 1:1 ratio in acetonitrile at room temperature. The reaction of CuI and $\mathbf{L^1}$ in acetonitrile forms **CP1** irrespective of the ratio of reactants, while with $\mathbf{L^2}$ and $\mathbf{L^3}$ formation of some unknown products was also observed in small amounts along with **CP2** and **CP3**, respectively, when different ratios of reactants were used. The multidentate ligands $\mathbf{L^1}$ and $\mathbf{L^2}$ afforded 1D coordination polymers, while $\mathbf{L^3}$ led to a 2D **CP3** (**Scheme 1**). Crystals suitable for single crystal X-ray diffraction (SC-XRD) analysis were obtained by slow evaporation of the acetonitrile solutions of **CP1** and **CP2** at room temperature. The room temperature reaction of $\mathbf{L^3}$ with CuI and KI also yielded **CP3** and crystals of **CP3** were obtained by the slow diffusion of an ethanol solution of $\mathbf{L^3}$ to an aqueous solution containing KI and CuI. The purity of the bulk samples was confirmed by comparing the powder X-ray diffraction (PXRD) data with the simulated PXRD pattern obtained from SC-XRD analysis (**Fig. S6-S8**). Infra-red (IR) spectra of all the ligands and CPs are presented in **Fig S9-S14**. The bands in the range 1586-1450- cm^{-1} correspond to the stretching frequencies of C-C and C-N of the pyridyl ring, and the weak bands at 1399-1275 cm^{-1} correspond to the N-N and C-N stretching frequencies of the triazole ring of $\mathbf{L^1}$-$\mathbf{L^3}$**.** The corresponding stretching frequencies in **CP1**-**CP3** are significantly shifted, suggesting the coordination of the ligands to the metal.

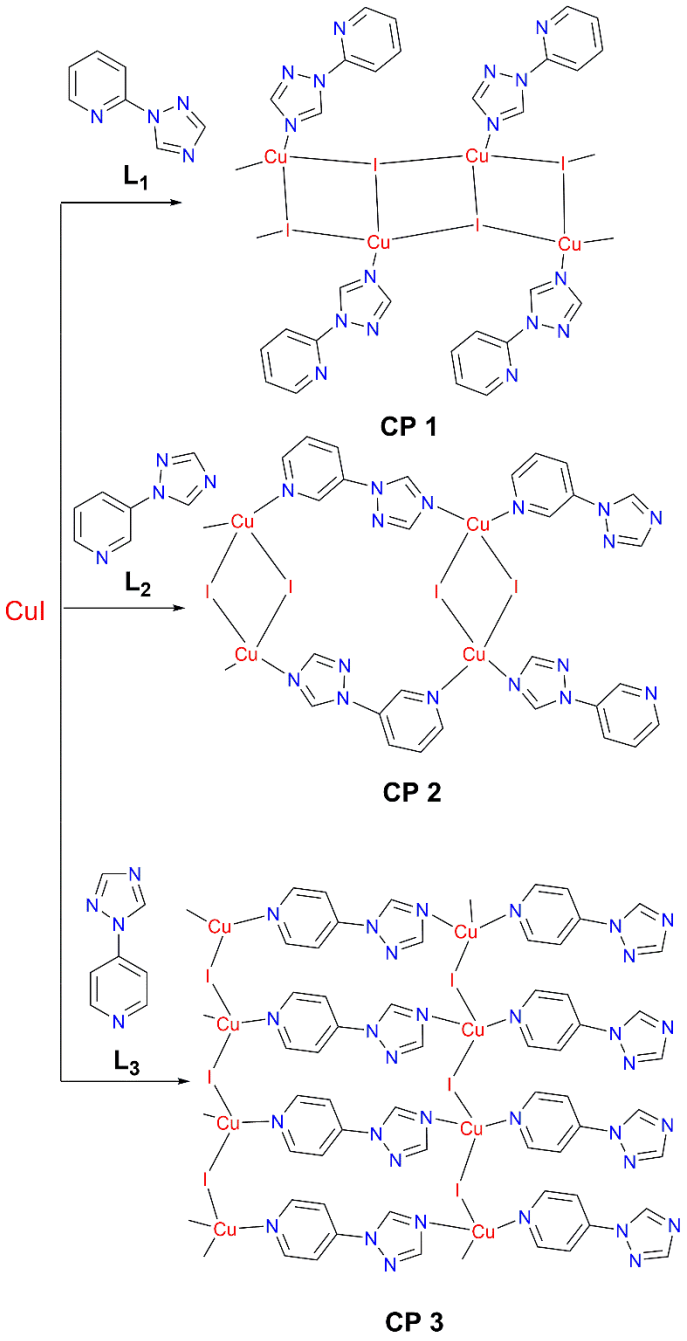

Scheme 1. Synthesis of CPs.

Structural analysis

Fig. 2. (a) Asymmetric unit of **CP1**, (b) 1-D coordination polymer **CP1** having Cu_2I_2 double chains.

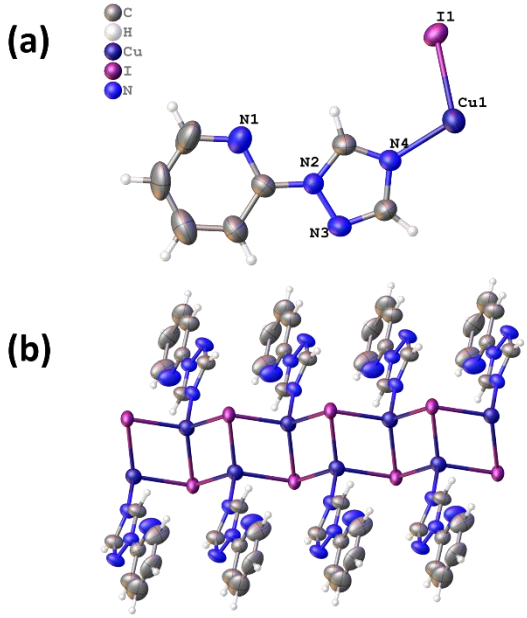

To get an insight into the atomic arrangement in the coordination polymer, SC-XRD data was recorded from the needle-shaped crystals of **CP1**. **CP1** crystallizes in a monoclinic system in a *P2₁/c* space group having a polymeric double chain like a staircase (**Fig. 2**). The asymmetric unit contains one copper, one iodide atom and one $\mathbf{L^1}$ ligand. The coordination of each copper atom

in the infinite double chain is satisfied by three μ_3-I and one nitrogen of 1,2,4-triazole unit, forming a distorted tetrahedral geometry around copper and a distorted pyramidal geometry around the iodide atom. The geometry around copper can be best described by calculating the angular index (τ_4) ($\tau_4 = [360 - (a + b)]/141$ where a and b are the two largest angles around the copper atom), which is 0.94, confirming the distorted tetrahedral geometry.[49] The density of the **CP1's** crystal (d_{calc}=2.339 g cm^{-3}) is close to those previously reported for other polymers.[50–52] The crystal structure reveals no significant interactions between the 1D chains except some weak C-H---N (2.54-2.67 Å) and C-H---I (3.078 Å) interactions (**Fig. S3**). Despite having three coordination centres (one pyridyl nitrogen and two triazolyl nitrogen), only one triazolyl nitrogen was found coordinated to copper with a Cu–N4 distance of 2.038(7) Å, which is in the range of similarly reported polymers.[53,54] In the $\{Cu_2(\mu_3\text{-}I)_2\}_n$ infinite 1D ladder, the Cu–Cu distances on the alternate unit are significantly different; one is shorter (dCu1–Cu1^2 = 2.750(3) Å) while the other one is longer (dCu1–Cu1^1=2.900(2) Å), along the symmetry operation code (1) -*x*, 1-*y*, -*z* and (2) -*x*, 1-*y*, -*z*. The two ligands coordinated to the copper centre adjacent to each other are arranged parallelly, and the centroid distance between the adjacent pyridine or triazole rings is 4.187 Å.

The yellow crystals of **CP2** crystallize in a triclinic system with $P\bar{1}$ space group having one copper, one iodide and one [3-(1H-1,2,4triazol-1-yl)pyridine] unit in the asymmetric unit. The complete structure exhibits a discrete Cu_2I_2 rhomboid as a secondary building unit (SBU) bridges with $\mathbf{L^2}$**,** thus forming 1D **CP2** with an 18-membered metallacycle. The Cu_2I_2 SBU, unlike **CP1**, is connected with the pyridinic nitrogen from one side and triazolyl nitrogen from the other side with an inclination of 116.23 and 113.04° with the core unit, respectively, forming a 1D infinite chain (**Fig. 3**). The τ_4 value for **CP2** is 0.80, confirming the distorted tetrahedral geometry

around the metal centre. The centroid distance between the two opposite bridging rings is 5.227 Å. The Cu1-Cu1^{1} distance is 2.8478(14) Å, slightly longer than the sum of van der Waals radii along the symmetry operation code 1-*x*, 1-*y*, -*z*. The Cu1–N1^{1} and Cu1–N4 distances of 2.021(4) Å and 2.023(4) Å along the symmetry operation (1) 1-*x*, 1-*y*, -*z*, are almost similar despite the coordination of different *N*-donor rings. The volume calculated is 471.01(5) Å^{3}, nearly half of the volume of **CP1** (956.03(10) Å^{3}), due to the closed-ordered structure. The crystal structure reveals no significant interaction between the adjacent 1D chains except some weak C–H---N and C–H---I interactions with distances ranging from 2.696 Å to 3.091-3.164 Å (**Fig. S4**), respectively. A similar structure was also reported with 3-picolylamine [Cu_2I_2(3pica)], where the Cu_2I_2 core is perpendicular to the bridging atoms and Cu–Cu distance is slightly larger 3.086(3) Å.[36]

Fig. 3. (a) Asymmetric unit of **CP2** (b) schematic representation of the polymeric chain bridged by two rings (c) Cu_2I_2 core bridged by 3-(1H-1,2,4triazol-1-yl)pyridine in 1D-coordination polymer **CP2**.

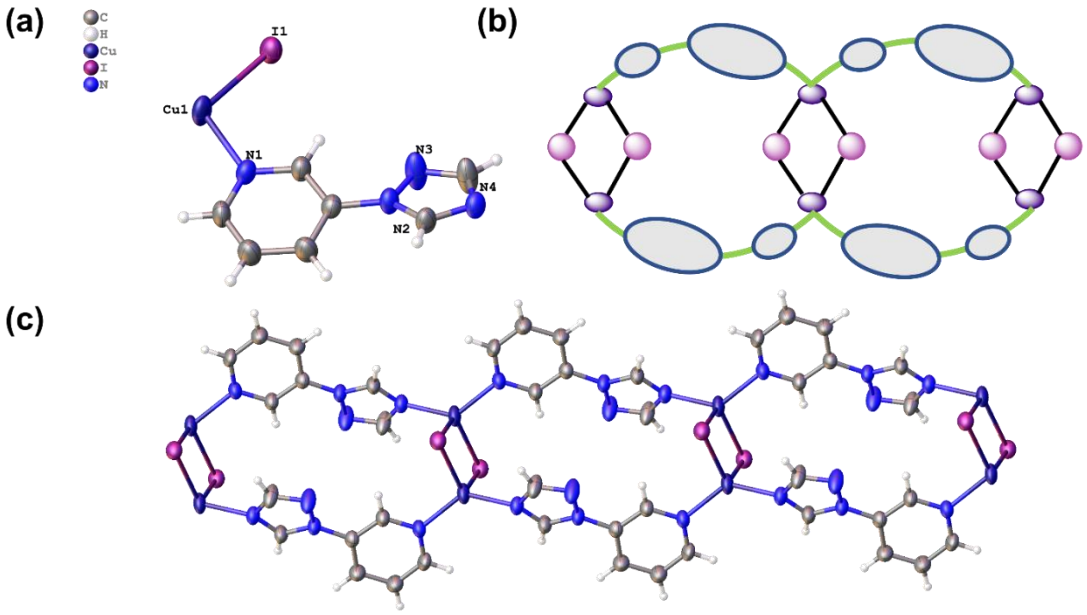

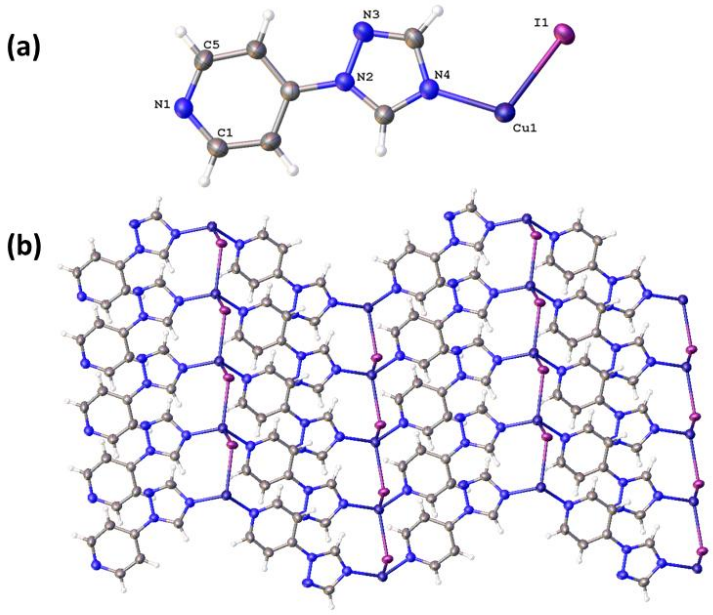

Fig. 4. (a) Asymmetric unit of **CP3**, (b) 2D **CP3** consisting of Cu-I single chain bridged by the 4-(1H-1,2,4triazol-1-yl)pyridine.

CP3 crystallizes in the monoclinic $P2_1/c$ space group with one copper, one iodide and one ligand in the asymmetric unit. Unlike **CP1** and **CP2**, the polymeric structure consists of zig-zag copper-iodide chains, where copper (I) atoms are bridged by two nitrogen atoms of $\mathbf{L}^{\mathbf{3}}$, forming a zig-zag polymeric 2D network (**Fig. 4**). Similar structure of 2D $[CuI(pyz)]_n$ comprising Cu–I zig-zag network bridged by pyrazine was also reported by Fonari *et al*.[55] N4 nitrogen of triazole and the nitrogen of the pyridine ring coordinated to copper atoms with Cu–N distance equal to 2.04 Å which is slightly larger than **CP1** and **CP2**. The τ_4 value for **CP3** is 0.93, suggesting the geometry around copper is distorted tetrahedral. The bond angles between Cu1–I1–$Cu1^1$ and I1–Cu1–$I1^2$ (108.115(17)°) are the same along the symmetry operation code (1) -1+*x*, + *y*,+ *z*, (2)1+*x*,+ *y*,+ *z*, respectively. The calculated density of **CP3** is 2.478 g cm^{-3}, slightly larger than **CP1** and **CP2**. The 2D assembly of ligands between the 1D Cu---I chains also constituted π- π

interactions between two triazolyl rings with a distance of 3.271 Å. Some weak C–H---I interactions were also observed and the distances between them are 3.746 Å (**Fig. S5**). A comparison of Cu–I, Cu–N and Cu–Cu distances of all the reported CPs are summarised in **Table 1**, while other details of bond lengths and bond angles are provided in **Table S2-S7**.

Table 1. Selected bond lengths (Å) for **CP1**, **CP2** and **CP3**.

Compound	Cu–I		Cu–N		Cu–Cu	
CP1	2.6466(15)	2.6639(14)	2.038(7)		2.900(2)	2.750(3)
CP2	2.6848(7)	2.7381(8)	2.021(4)	2.023(4)	2.8478(14)	
CP3	2.6478(5)	2.6796(5)	2.042(3)	2.043(3)	4.313	

Thermogravimetric analysis

TGA analyses have been performed to measure the stability of the polymers under N_2 flow (20 mL/ min) with an increase in temperature of 10 °C/ min (**Fig. S15-17**). A slight increase in weight between the temperature range 30-150 °C is observed due to the buoyancy effect. As the temperature increases, the density of the gas (fluid) decreases, resulting in a slight mass gain during the analysis. This effect is prominent in the lower temperature range, as the temperature increases, the buoyancy effect decreases. The first degradation step for **CP1** starts at 158 °C with a loss of approximately 42 %, corresponding to the complete dissociation of $\mathbf{L^1}$ molecule (**Fig. S15**). The second weight loss of 33 % corresponds to the loss of iodide from the cluster. Similarly, **CP2** (**Fig. S16**) and **CP3** (**Fig. S17**) show a first degradation of the ligands ($\mathbf{L^2}$) and ($\mathbf{L^3}$) from the cluster at a temperature of 183 and 194 °C, respectively and follow a similar trend

as **CP1**. TGA analysis confirms that **CP3** is the more stable among the reported CPs due to its 2D structure.

Photophysical study

The luminescence spectra of **CP1**, **CP2** and **CP3** were recorded at room temperature (298K) and 77K (**Fig. 5**). At room temperature, on excitation at 373 nm, **CP1** showed a broad emission band at 538 nm with a shoulder at 480 nm (**Fig. S18**). This suggests a dual emission originating from two different excited states, which is confirmed by the presence of biexponential lifetime of 85μs (τ1, 73 %) and 1.12ms (τ2, 27 %) with a quantum yield of 4.2 % (**Fig. S19**). Longer lifetime in the millisecond (ms) range is not unprecedented; recently, Lucia *et al.* have observed lifetime up to millisecond for a copper(I) iodide CP, i.e. $\{[CuIL]\cdot 0.5(I_2)\}_n$ (L = cyclic triimidazole).[53,56] The longer lifetime suggests the luminescence originates from a triplet state and can be assigned to phosphorescence. Further, the dual emission suggests overlapping low energy metal-cluster centre (^{3}CC) and high energy metal-halide to ligand charge transfer (^{3}M+I-LCT).[57] Several reports on CPs having *N* as a donor site confirms the origin of luminescence through both charge transfer states.[58–60] The occurrence of ^{3}CC charge transfer at 298K can also be established by the small Cu–Cu distance of 2.750 (3) Å. The plausible charge transfer process in **CP1** is presented in **Fig. 6**. The thermal energy at 298K is sufficient to populate the ^{3}CC state from the triplet (^{3}M+I-LCT) states. At lower temperatures, the thermal energy is not sufficient to populate the ^{3}CC state and only one band is observed, typically through (^{3}M+I-LCT).[61,62] Therefore, when the temperature decreases to 77K, the emission band corresponds to ^{3}CC subside, while (^{3}M+I-LCT) band dominates and the emission maxima is observed at 477 nm.

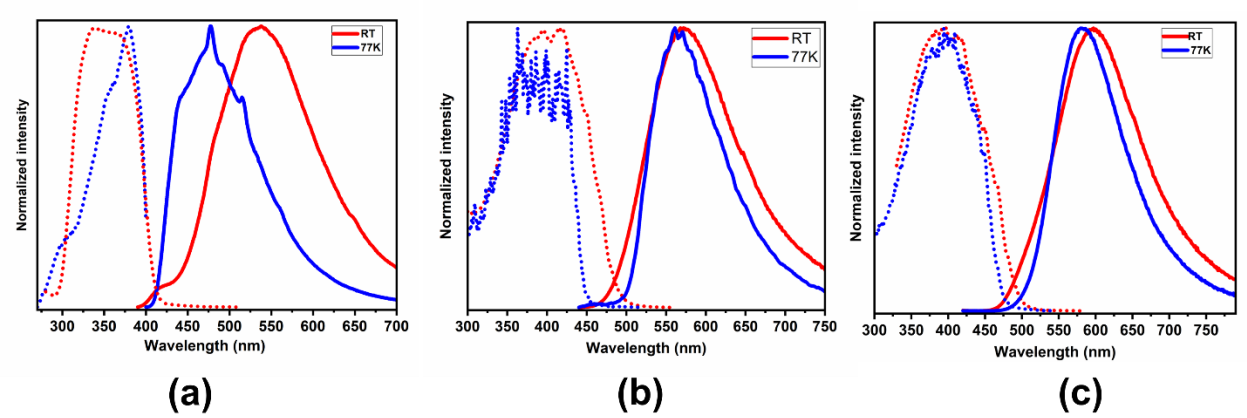

Fig. 5. Normalized excitation (dotted line) at rt (red) and 77K (blue) and emission spectra (solid line) at rt (red) and 77K (blue) for **CP1 (a)**, **CP2 (b)** and **CP3 (c)**.

At room temperature, the luminescence spectrum of **CP2** presents an emission maximum at 575 nm on excitation at 420 nm with a decay time of 6.96 μs with photoluminescence quantum yield Φ =3.7% (**Fig. S20**). In contrast to **CP1**, only a slight blue shift of the emission band (Δλ = 11 nm) is observed upon cooling to 77K, suggesting no geometrical distortion due to the structural rigidity of the CP.[36,57,63]. Lang *et al.* reported a similar Cu_2I_2 rhomboid containing CP $[CuI(bpp)]_n$ with pyridine-containing ligands having a room temperature emission.[64] Similar complexes [CuI(3pica] and [CuI(3pica)]CH_3CN were reported by Maini *et al.*, where also no emission change was observed on lowering the temperature due to less geometrical distortion.[36] The large Cu–Cu distance (2.8478(14) Å) rule out the contribution of ^{3}CC to the emission spectrum. Therefore at 298K, the microsecond lifetime suggests the involvement of ^{3}(M+I-LCT) state.

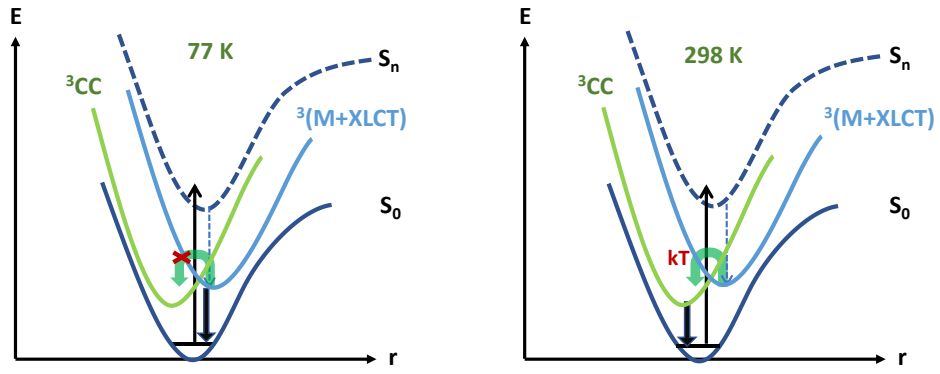

Fig. 6. Schematic representation of charge transfer through Jablonski diagram for **CP1** at 77K and 298K.

The emission spectrum of **CP3** shows a broad band at 600 nm on excitation at 400 nm at room temperature having lower quantum yield (Φ =0.7%) compared to **CP1** and **CP2** (**Fig. S21**). The lifetime of 12 microseconds at room temperature suggests the phosphorescence originating from ^{3}(M+I-LCT). At 77K, the emission maximum is 42 nm blue-shifted as in **CP1**. However, the absence of any cluster (*d*Cu–Cu = 4.31 Å) and monoexponential lifetime confirms no cluster-centered emission. Fonari *et*. *al* have reported similar 2D CPs with pyrazine as a ligand exhibiting red-shift at 77K due to thermally activated delayed fluorescence.[55] Probably, the smaller Cu–I bond distances at lower temperature leads to the stabilization of the ground state and could be responsible for the blue-shifted emission in **CP3**. A comparison of photophysical parameters for all our CPs are summarised in **Table 2**.

Table 2. Photophysical properties of **CP1**, **CP2** and **CP3**.

CP	Excitation (nm), 298K	Excitation (nm), 77K	Emission (nm), 298K	Emission (nm), 77K	Quantum Yield, Φ (%) 300K	Lifetime, 298K

CP1	373	380	538	477	4.2	τ1 (85 µs; 73 %), τ2 (1.12 ms, 27 %)
CP2	420	420	575	564	3.7	τ (6.96 µs 99.97 %)
CP3	400	400	600	580	0.7	τ2 (12 µs; 99 %), τ1 (238 µs; 1 %)

Electrical conductivity

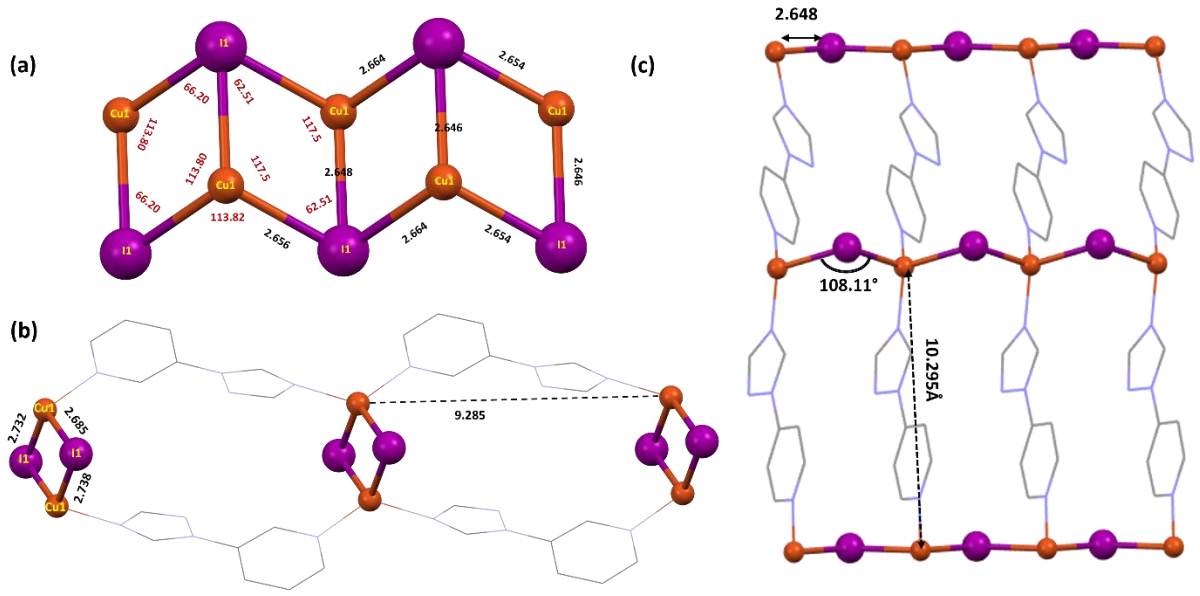

Zamora and co-workers have reported the semiconducting properties of various CuI CPs. They

Fig. 7. (a) Relevant geometrical parameters of electrical conductivities for (a) **CP1**, (b) **CP2** and (c) **CP3**

have shown that the resistivity of copper(I) CPs can be measured using single crystals or pressed pellets using the two-probe or four-probe method. Conductivity values in the range of 10 S cm^{-1}-

10^5 S cm^{-1} correspond to metallic compounds, those in the range of 10^{-10} S cm^{-1}- 10 S cm^{-1} to semiconductors and lower values correspond to insulators.[65,66]

The electrical conductivity values of the three synthesized CPs have been recorded using the two-probe direct current method at 300K on pressed pellets (5.0 GPa, 5 min). To perform the experiment, Keithley model 6517B electrometer voltage source was used and silver paste was applied to contact the pressed pellets. The conductivity values of all the CPs were obtained by applying voltages ranging from -10 V to +10 V. Conductivity values of 8.85×10^{-7} S cm^{-1}, 6.73×10^{-8} S cm^{-1} and 3.42×10^{-7} S cm^{-1} were found for **CP1**, **CP2** and **CP3**, respectively (**Fig. S22-24**), suggesting the semiconductor nature of the synthesized CPs. All the structures are different, and we cannot directly compare their electrical properties to each other. In the 1D **CP1**, charge propagation occurs through the Cu_2I_2 double chain; in **CP2**, it is through the bridging organic ligand and rhomboid Cu_2I_2. In 2D **CP3**, two possible pathways exist for electronic delocalization (i) Cu-I-Cu zig-zag chain and (ii) Cu-L^3-Cu connections.[67] The electrical conductivity of these CPs can be explained based on their structural arrangements consisting of Cu-Cu bond distances and Cu-I-Cu and I-Cu-I bond angles (**Fig. 7**), which results in better overlapping of orbitals for the propagation of charge carriers.[66] Average Cu-Cu bond distances are approximately 2.825 Å in **CP1**, slightly smaller than 2.848 Å in **CP2**. The average Cu-I bond lengths are 2.654 Å, 2.735 Å and 2.664 Å and the I-Cu-I bond angles are 110.65° (average), 116.66(3)° and 108.115(17)° for **CP1**, **CP2** and **CP3**, respectively. Larger I-Cu-I bond angles and smaller Cu-I distances lead to better overlapping between the d_z^2 orbital on the metal and the p_z orbitals on the iodide leading to better electrical conductivity.[68] Though **CP2** has the largest I-Cu-I bond angle, the smallest Cu-I distance along with Cu_2I_2 rhomboids, this CP presents the lowest conductivity value. Oppositely, **CP1** and **CP3** with the lowest I-Cu-I bond angle, shortest Cu-I distance and a

continuous Cu_2I_2 double chain or Cu-I continuous chain, present better electrical conductivity than **CP2**. Among these two CPs, **CP1** shows the highest electrical conductivity value because of the continuous Cu_2I_2 stair motif propagating along the axes, which helps in more efficient transportation of electrons than in **CP3** with comparatively less orbital overlap. Pilar Amo-Ochoa *et al*. reported that $[Cu_2I_2(Fpyz)]_n$ and $[Cu(Cl\text{-}HIN)I]_n$ CPs having Cu_2I_2 chains present better conductivity ($\sigma \sim 10^{-5}$ S cm^{-1}) than **CP1**.[69,70] Some previously reported Cu(I) CPs, having Cu_2I_2 double chain, similar to **CP1**, have been reported to show electrical conductivity in the similar range.[68,71–74] A comparison of electrical conductivities of **CP1** with some previously reported CPs bearing Cu_2I_2 core is presented in **Table S8**, suggesting comparable values for **CP1**. However, we could not find any report of electrical conductivity measurements for CPs with similar structure to **CP2** and **CP3**.

Conclusion

We have reported 1D **CP1** and **CP2** by reacting CuI with $\mathbf{L^1}$ and $\mathbf{L^2}$, whereas 2D **CP3** was obtained with $\mathbf{L^3}$. The temperature-dependent excitation and emission spectra were recorded in solid-state at room temperature and 77K. The room temperature emission of **CP1** is green (λ_{em} = 538 nm), yellow (λ_{em} = 575 nm) for **CP2** and orange (λ_{em} = 600 nm) for **CP3**. On lowering the temperature to 77K, the emission of **CP1** shifted to blue (λ_{em} = 477 nm), and the emission of **CP3** shifted to yellow (λ_{em} = 562 nm)**,** while no significant change was observed for **CP2**. The emissions can thus cover almost the whole visible spectrum from blue-orange depending on the temperature for different CPs. The lifetime experiment showed dual phosphorescence for **CP1,** indicating the origin of luminescence via ^{3}CC and (^{3}M+I-LCT). The emission and microsecond lifetime at room temperature for **CP2** and **CP3** originated from (^{3}M+I-LCT). The electrical conductivities of these polymers were also recorded and found within the range of 10^{-7} to 10^{-8} S

cm^{-1} suggesting semiconductor behaviour. **CP1** showed a higher electrical conductivity value of $\sigma = 8.85 \times 10^{-7}$ S cm^{-1} than **CP3** ($\sigma = 3.42 \times 10^{-7}$ S cm^{-1}) due to comparatively better orbital overlap between Cu (d_z^2) and I (p_z); while, **CP2** has the lowest conductivity value of $\sigma = 6.73 \times 10^{-8}$ S cm^{-1}. The structural features help us to evaluate the photophysical and electrical properties. In conclusion, this work has demonstrated that, the coordination to CuI of structural isomeric ligands could result into different coordination polymers with significantly different properties. Further, the desired photophysical and conducting properties could be achieved by carefully tuning the ligands and SBUs. In addition, the luminescence of the resulting CPs can be tuned by using different ancillary ligands. The synthesized triazole-based CPs could be useful for application in thermochromic sensor or molecular thermometer. We are currently exploring the application of the reported CPs and similar CPs for sensing various volatile organic solvents and gases.

Acknowledgment

S.M. and D.P. are grateful to IIT Indore for the fellowship. Sophisticated instrumentation centre (SIC) IIT Indore and the Department of Chemistry IIT Indore are acknowledged for providing characterization facilities. We thank Prof. Preeti A. Bhobe (Department of Physics, IIT Indore) for providing the electrical conductivity facility Dr. Abhijit Patra, Department of Chemistry, Indian Institute of Science Education and Research, Bhopal (IISERB) for quantum yield measurements and Dr. Kuldeep Mahiya for helping with the structural solution and refinement for CP1.

Conflicts of interest

The Authors declare no conflict of interest.

References

1 W. Liu, Y. Fang and J. Li, *Advanced Functional Materials*, 2018, **28**, 1705593.
2 T. Hayashi, A. Kobayashi, H. Ohara, M. Yoshida, T. Matsumoto, H.-C. Chang and M. Kato, *Inorg. Chem.*, 2015, **54**, 8905–8913.
3 R. Czerwieniec, M. J. Leitl, H. H. H. Homeier and H. Yersin, *Coordination Chemistry Reviews*, 2016, **325**, 2–28.
4 E. Cariati, E. Lucenti, C. Botta, U. Giovanella, D. Marinotto and S. Righetto, *Coordination Chemistry Reviews*, 2016, **306**, 566–614.
5 H. Li, Y. Lv, Z. Zhou, H. Tong, W. Liu and G. Ouyang, *Angewandte Chemie*, 2022, **134**, e202115225.
6 A. V. Artem'ev, E. P. Doronina, M. I. Rakhmanova, O. A. Tarasova, I. Y. Bagryanskaya and N. A. Nedolya, *Inorg. Chem. Front.*, 2019, **6**, 671–679.
7 Y.-L. Wang, X.-Y. Li, S.-D. Han, J. Pan and Z.-Z. Xue, *Crystal Growth & Design*, 2022, **22**, 3719–3726.
8 J. Troyano, J. Perles, P. Amo-Ochoa, J. I. Martínez, F. Zamora and S. Delgado, *CrystEngComm*, 2014, **16**, 8224–8231.
9 Y.-D. Lin, C.-W. Lu and H.-C. Su, *Chemistry – A European Journal*, 2023, **29**, e202202985.
10 V. K.-M. Au, *Energy Fuels*, 2021, **35**, 18982–18999.
11 J. López-Molino and P. Amo-Ochoa, *ChemPlusChem*, 2020, **85**, 1564–1579.
12 E. Fresta, M. D. Weber, J. Fernandez-Cestau and R. D. Costa, *Advanced Optical Materials*, 2019, **7**, 1900830.
13 G. H. Morritt, H. Michaels and M. Freitag, *Chem. Phys. Rev.*, 2022, **3**, 011306.
14 M. Olaru, E. Rychagova, S. Ketkov, Y. Shynkarenko, S. Yakunin, M. V. Kovalenko, A. Yablonskiy, B. Andreev, F. Kleemiss, J. Beckmann and M. Vogt, *J. Am. Chem. Soc.*, 2020, **142**, 373–381.
15 K. Tsuge, Y. Chishina, H. Hashiguchi, Y. Sasaki, M. Kato, S. Ishizaka and N. Kitamura, *Coordination Chemistry Reviews*, 2016, **306**, 636–651.
16 N. Robertson and L. Cronin, *Coordination Chemistry Reviews*, 2002, **227**, 93–127.
17 J. Troyano, F. Zamora and S. Delgado, *Chem. Soc. Rev.*, 2021, **50**, 4606–4628.
18 A. Schlachter, K. Tanner and P. D. Harvey, *Coordination Chemistry Reviews*, 2021, **448**, 214176.
19 J. Conesa-Egea, F. Zamora and P. Amo-Ochoa, *Coordination Chemistry Reviews*, 2019, **381**, 65–78.
20 Y. Liu, S.-C. Yiu, C.-L. Ho and W.-Y. Wong, *Coordination Chemistry Reviews*, 2018, **375**, 514–557.
21 Y. Zhang, M. Schulz, M. Wächtler, M. Karnahl and B. Dietzek, *Coordination Chemistry Reviews*, 2018, **356**, 127–146.
22 W. Liu, Y. Fang, G. Z. Wei, S. J. Teat, K. Xiong, Z. Hu, W. P. Lustig and J. Li, *J. Am. Chem. Soc.*, 2015, **137**, 9400–9408.
23 S. Masahara, H. Yokoyama, Y. Suzaki and T. Ide, *Dalton Trans.*, 2021, **50**, 8889–8898.
24 S. Henfling, R. Kempt, J. Klose, A. Kuc, B. Kersting and H. Krautscheid, *Inorg. Chem.*, 2020, **59**, 16441–16453.
25 A. Schlachter, K. Tanner, R. Scheel, P.-L. Karsenti, C. Strohmann, M. Knorr and P. D. Harvey, *Inorg. Chem.*, 2021, **60**, 13528–13538.
26 Q. Benito, X. F. Le Goff, G. Nocton, A. Fargues, A. Garcia, A. Berhault, S. Kahlal, J.-Y. Saillard, C. Martineau, J. Trébosc, T. Gacoin, J.-P. Boilot and S. Perruchas, *Inorg. Chem.*, 2015, **54**, 4483–4494.

27 S. Kumar, D. Mondal and M. S. Balakrishna, *ACS Omega*, 2018, **3**, 16601–16614.
28 Y. Fang, W. Liu, S. J. Teat, G. Dey, Z. Shen, L. An, D. Yu, L. Wang, D. M. O'Carroll and J. Li, *Advanced Functional Materials*, 2017, **27**, 1603444.
29 C. Chen, R.-H. Li, B.-S. Zhu, K.-H. Wang, J.-S. Yao, Y.-C. Yin, M.-M. Yao, H.-B. Yao and S.-H. Yu, *Angewandte Chemie International Edition*, 2018, **57**, 7106–7110.
30 R. Utrera-Melero, B. Huitorel, M. Cordier, F. Massuyeau, J.-Y. Mevellec, N. Stephant, P. Deniard, C. Latouche, C. Martineau-Corcos and S. Perruchas, *J. Mater. Chem. C*, 2021, **9**, 7991–8001.
31 S. Perruchas, *Dalton Trans.*, 2021, **50**, 12031–12044.
32 Y. Wu, J.-Y. Wang, L.-Y. Zhang, L.-J. Xu and Z.-N. Chen, *Inorg. Chem.*, 2020, **59**, 17415–17420.
33 A. Kobayashi and M. Kato, *Chem. Lett.*, 2017, **46**, 154–162.
34 S. Tunsrichon, K. Chainok, V. Promarak, P. Nalaoh, S. Youngme and J. Boonmak, *Inorg. Chem.*, 2022, **61**, 11734–11745.
35 H. D. Hardt and A. Pierre, *Inorganica Chimica Acta*, 1977, **25**, L59–L60.
36 F. Farinella, L. Maini, P. P. Mazzeo, V. Fattori, F. Monti and D. Braga, *Dalton Trans.*, 2016, **45**, 17939–17947.
37 R. Hamze, J. L. Peltier, D. Sylvinson, M. Jung, J. Cardenas, R. Haiges, M. Soleilhavoup, R. Jazzar, P. I. Djurovich, G. Bertrand and M. E. Thompson, *Science*, 2019, **363**, 601–606.
38 N. Kitada and T. Ishida, *CrystEngComm*, 2014, **16**, 8035–8040.
39 A.-N. Dou, Y.-C. Du, Q.-L. Chen, K.-L. Luo, C. Zhang, A.-X. Zhu and Q.-X. Li, *Zeitschrift für anorganische und allgemeine Chemie*, 2016, **642**, 731–735.
40 B. Li, Y. Peng, G. Li, J. Hua, Y. Yu, D. Jin, Z. Shi and S. Feng, *Crystal Growth & Design*, 2010, **10**, 2192–2201.
41 Y.-L. Wang, N. Zhang, Q.-Y. Liu, Z.-M. Shan, R. Cao, M.-S. Wang, J.-J. Luo and E.-L. Yang, *Crystal Growth & Design*, 2011, **11**, 130–138.
42 A. Gusev, M. Kiskin, E. Braga, E. Zamnius, M. Kryukova, N. Karaush-Karmazin, G. Baryshnikov, B. Minaev and W. Linert, *RSC Advances*, 2023, **13**, 3899–3909.
43 D. M. Zink, D. Volz, T. Baumann, M. Mydlak, H. Flügge, J. Friedrichs, M. Nieger and S. Bräse, *Chem. Mater.*, 2013, **25**, 4471–4486.
44 M. Grupe, P. Boden, P. Di Martino-Fumo, X. Gui, C. Bruschi, R. Israil, M. Schmitt, M. Nieger, M. Gerhards, W. Klopper, C. Riehn, C. Bizzarri and R. Diller, *Chemistry – A European Journal*, 2021, **27**, 15252–15271.
45 C. Bizzarri, A. P. Arndt, S. Kohaut, K. Fink and M. Nieger, *Journal of Organometallic Chemistry*, 2018, **871**, 140–149.
46 N. Kommu, V. D. Ghule, A. S. Kumar and A. K. Sahoo, *Chemistry – An Asian Journal*, 2014, **9**, 166–178.
47 N. V. Shevchuk, K. Liubchak, K. G. Nazarenko, A. A. Yurchenko, D. M. Volochnyuk, O. O. Grygorenko and A. A. Tolmachev, *Synthesis*, 2012, **44**, 2041–2048.
48 J.-C. Li, H.-X. Li, H.-Y. Li, W.-J. Gong and J.-P. Lang, *Crystal Growth & Design*, 2016, **16**, 1617–1625.
49 S. Tunsrichon, K. Chainok, V. Promarak, P. Nalaoh, S. Youngme and J. Boonmak, *Inorg. Chem.*, 2022, **61**, 11734–11745.
50 J.-C. Li, H.-X. Li, H.-Y. Li, W.-J. Gong and J.-P. Lang, *Crystal Growth & Design*, 2016, **16**, 1617–1625.
51 S. Tunsrichon, K. Chainok, V. Promarak, P. Nalaoh, S. Youngme and J. Boonmak, *Inorg. Chem.*, 2022, **61**, 11734–11745.
52 A. V. Artem'ev, M. I. Rakhmanova and D. G. Samsonenko, *J Struct Chem*, 2019, **60**, 617–622.
53 E. Lucenti, E. Cariati, A. Previtali, D. Marinotto, A. Forni, V. Bold, V. Ch. Kravtsov, M. S. Fonari, S. Galli and L. Carlucci, *Crystal Growth & Design*, 2019, **19**, 1567–1575.

54 H. Zhao, X. Li, J. Wang, L. Li and R. Wang, *ChemPlusChem*, 2013, **78**, 1491–1502.
55 I. L. Malaestean, V. Ch. Kravtsov, J. Lipkowski, E. Cariati, S. Righetto, D. Marinotto, A. Forni and M. S. Fonari, *Inorg. Chem.*, 2017, **56**, 5141–5151.
56 D. Malpicci, E. Lucenti, A. Forni, D. Marinotto, A. Previtali, L. Carlucci, P. Mercandelli, C. Botta, S. Righetto and E. Cariati, *Inorg. Chem. Front.*, 2021, **8**, 1312–1323.
57 P. Boden, P. Di Martino-Fumo, J. M. Busch, F. R. Rehak, S. Steiger, O. Fuhr, M. Nieger, D. Volz, W. Klopper, S. Bräse and M. Gerhards, *Chemistry – A European Journal*, 2021, **27**, 5439–5452.
58 J. López, J. G. Platas, U. R. Rodríguez-Mendoza, J. I. Martínez, S. Delgado, G. Lifante-Pedrola, E. Cantelar, R. Guerrero-Lemus, C. Hernández-Rodríguez and P. Amo-Ochoa, *Inorg. Chem.*, 2021, **60**, 1208–1219.
59 C. Tard, S. Perruchas, S. Maron, X. F. Le Goff, F. Guillen, A. Garcia, J. Vigneron, A. Etcheberry, T. Gacoin and J.-P. Boilot, *Chem. Mater.*, 2008, **20**, 7010–7016.
60 D. M. Zink, D. Volz, T. Baumann, M. Mydlak, H. Flügge, J. Friedrichs, M. Nieger and S. Bräse, *Chem. Mater.*, 2013, **25**, 4471–4486.
61 J. López, M. Murillo, G. Lifante-Pedrola, E. Cantelar, J. Gonzalez-Platas, U. R. Rodríguez-Mendoza and P. Amo-Ochoa, *CrystEngComm*, 2022, **24**, 341–349.
62 K. A. Vinogradova, N. A. Shekhovtsov, A. S. Berezin, T. S. Sukhikh, M. I. Rogovoy, A. V. Artem'ev and M. B. Bushuev, *Dalton Transactions*, 2021, **50**, 9317–9330.
63 A. J. Lees, *Comments on Inorganic Chemistry*, 1995, **17**, 319–346.
64 Y. Chen, H.-X. Li, D. Liu, L.-L. Liu, N.-Y. Li, H.-Y. Ye, Y. Zhang and J.-P. Lang, *Crystal Growth & Design*, 2008, **8**, 3810–3816.
65 G. Givaja, P. Amo-Ochoa, C. J. Gómez-García and F. Zamora, *Chemical Society Reviews*, 2012, **41**, 115–147.
66 P. Amo-Ochoa, K. Hassanein, C. J. Gómez-García, S. Benmansour, J. Perles, O. Castillo, J. I. Martínez, P. Ocón and F. Zamora, *Chem. Commun.*, 2015, **51**, 14306–14309.
67 J. Troyano, J. Perles, P. Amo-Ochoa, F. Zamora and S. Delgado, *CrystEngComm*, 2016, **18**, 1809–1817.
68 K. Hassanein, J. Conesa-Egea, S. Delgado, O. Castillo, S. Benmansour, J. I. Martínez, G. Abellán, C. J. Gómez-García, F. Zamora and P. Amo-Ochoa, *Chemistry – A European Journal*, 2015, **21**, 17282–17292.
69 M. Murillo, R. Wannemacher, J. Cabanillas-González, U. R. Rodríguez-Mendoza, J. Gonzalez-Platas, A. Liang, R. Turnbull, D. Errandonea, G. Lifante-Pedrola, A. García-Hernán, J. I. Martínez and P. Amo-Ochoa, *Inorg. Chem.*, 2023, **62**, 10928–10939.
70 J. Conesa-Egea, Carlos. D. Redondo, J. I. Martínez, C. J. Gómez-García, Ó. Castillo, F. Zamora and P. Amo-Ochoa, *Inorg. Chem.*, 2018, **57**, 7568–7577.
71 J. Conesa-Egea, J. Gallardo-Martínez, S. Delgado, J. I. Martínez, J. Gonzalez-Platas, V. Fernández-Moreira, U. R. Rodríguez-Mendoza, P. Ocón, F. Zamora and P. Amo-Ochoa, *Small*, 2017, **13**, 1700965.
72 P. Amo-Ochoa, K. Hassanein, C. J. Gómez-García, S. Benmansour, J. Perles, O. Castillo, J. I. Martínez, P. Ocón and F. Zamora, *Chem. Commun.*, 2015, **51**, 14306–14309.
73 J. López, M. Murillo, G. Lifante-Pedrola, E. Cantelar, J. Gonzalez-Platas, U. R. Rodríguez-Mendoza and P. Amo-Ochoa, *CrystEngComm*, 2022, **24**, 341–349.
74 M. Murillo, J. Álvarez-Conde, R. Wannemacher, J. Cabanillas-González, J. González-Platas, U. R. Rodríguez-Mendoza, A. Liang, R. Turnbull, D. Errandonea, J. I. Martínez and P. Amo-Ochoa, *J. Mater. Chem. C*, 2022, **10**, 18004–18016.